Structure
Article

Structure of a Copper Pump Suggests a Regulatory Role for Its Metal-Binding Domain

Chen-Chou Wu,[1] William J. Rice,[2] and David L. Stokes[1,2,*]
[1]Skirball Institute of Biomolecular Medicine, School of Medicine, New York University, 540 First Avenue, New York, NY 10016, USA
[2]New York Structural Biology Center, 89 Convent Avenue, New York, NY 10027, USA
*Correspondence: stokes@nyu.edu
DOI 10.1016/j.str.2008.02.025

SUMMARY

P-type ATPases play an important role in Cu homeostasis, which provides sufficient Cu for metalloenzyme biosynthesis but prevents oxidative damage of free Cu to the cell. The P_{IB} group of P-type ATPases includes ATP-dependent pumps of Cu and other transition metal ions, and it is distinguished from other family members by the presence of N-terminal metal-binding domains (MBD). We have determined structures of two constructs of a Cu pump from *Archaeoglobus fulgidus* (CopA) by cryoelectron microscopy of tubular crystals, which reveal the overall architecture and domain organization of the molecule. By comparing these structures, we localized its N-terminal MBD within the cytoplasmic domains that use ATP hydrolysis to drive the transport cycle. We have built a pseudoatomic model by fitting existing crystallographic structures into the cryoelectron microscopy maps for CopA, which suggest a Cu-dependent regulatory role for the MBD.

INTRODUCTION

Copper is an essential cofactor for many enzymes but can be toxic because of its potential to drive oxidation/reduction reactions and to form free radicals. Therefore, all living cells from bacteria to mammals have developed mechanisms to finely control intracellular Cu concentration (Vulpe and Packman, 1995). P-type ATPases compose one of the principal protein families involved in Cu homeostasis, which include various ATP-dependent, transmembrane ion pumps, and has been divided into a number of subgroups, denoted P_I–P_V (Axelsen and Palmgren, 1998). Cu transport is handled by the P_{IB} group, which also includes transporters of other transition metal ions, such as Zn^{2+}, Cd^{2+}, Co^{2+}, and Pb^{2+} (Lutsenko and Kaplan, 1995; Williams and Mills, 2005). The best characterized P-type ATPases come from the P_{II} group and include mammalian Ca^{2+} ATPase and Na^+/K^+ ATPase, which have been the subject of numerous cell biological, biochemical, and structural studies (Kuhlbrandt, 2004).

In humans, two P_{IB} ATPases are responsible for maintaining appropriate Cu concentrations and, when defective, give rise to Menkes (MNK) and Wilson's (WNDP) diseases (DiDonato and Sarkar, 1997). They are found in the membrane of the trans-Golgi network but can be targeted to different cellular membranes in response to various cellular signals (Lutsenko et al., 2007). In yeast, Ccc2p pumps Cu into the Golgi (Yuan et al., 1997), and homologs have also been characterized from plants to bacteria—for example, OsHMA9 in *O. sativa* (Lee et al., 2007), CUA-1 in *C. elegans* (Yoshimizu et al., 1998), and either CopA or CopB in various bacteria (Mandal et al., 2002; Odermatt et al., 1993; Rensing et al., 2000). In most cases, soluble metallochaperones have also been identified, which play a role in chelating free Cu in the cytoplasm and delivering it to the transporters (Pufahl et al., 1997).

Members of the P-type ATPase family are characterized by the formation of a phosphorylated intermediate during the enzymatic cycle, by a common membrane topology and domain organization, and by conserved sequence motifs implicated in ATP hydrolysis and phosphorylation (Kuhlbrandt, 2004; Moller et al., 1996). Based primarily on studies of P_{II} ATPases, the reaction cycle involves alternation between E1 and E2 states, in which transmembrane ion sites are oriented toward the intracellular or extracellular milieu, respectively. A catalytic aspartate within the cytoplasmic domains can be phosphorylated in either state, which has a long-range conformational effect on the transmembrane domain and thus modulates accessibility of the ion transport sites therein. X-ray structures of the sarcoplasmic reticulum Ca^{2+} ATPase (SERCA1a) have defined three cytoplasmic domains and demonstrated the conformational changes that accompany principle steps of enzymatic cycle (Moller et al., 2005; Toyoshima and Inesi, 2004). In particular, the N domain binds ATP, the P domain contains the catalytic aspartate, and the A domain helps couple phosphorylation/dephosphorylation with ion site gating. P_{IB} ATPases retain these characteristics and are additionally equipped with a specialized N-terminal domain that carries characteristic metal-binding domains (MBD). Although there are several atomic structures of P_{IB} ATPases, they all represent isolated cytoplasmic domains—that is, N domain (Dmitriev et al., 2006; Haupt et al., 2004), composite N and P domain (Lubben et al., 2007; Sazinsky et al., 2006b), A domain (Sazinsky et al., 2006a), and N-terminal MBDs (Banci et al., 2002a, 2002b, 2004; Gitschier et al., 1998). To date, there is no structural information for an intact P_{IB} ATPase to elucidate the interaction of the MBDs with the rest of the molecule.

As many as six MBDs are arranged in tandem on the N-terminal tail of P_{IB} ATPases, which have a conserved sequence motif (GMTCxxC) and structural fold also found in the soluble metallochaperones (Arguello et al., 2007). The role of these MBDs is uncertain, though there is evidence for their contribution to protein targeting in mammalian cells (Forbes et al., 1999; Petris et al., 1996; Schaefer et al., 1999) and to regulation of transport activity (Huster and Lutsenko, 2003). Their structural homology to soluble

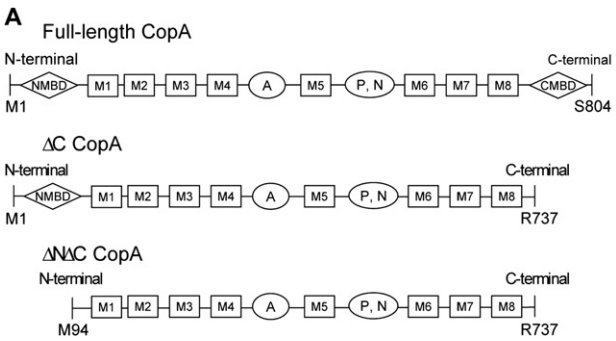

Figure 1. Constructs of CopA Used for Crystallization

(A) Domain organization of constructions with MBDs (◇), transmembrane helices (□), and cytoplasmic domains (○). Residues at the beginning and end of each construct are indicated, with ΔC-CopA and ΔNΔC-CopA used for crystallization.

(B) Coomassie-stained SDS polyacrylamide gel of the purified protein used for crystallization.

Cu^+ metallochaperones has led to the idea that MBDs mediate transfer of Cu^+ from chaperone to the transport site on the pump. Although transport has been demonstrated between metallochaperones and MBDs (Achila et al., 2006), no definitive evidence exists for transfer to the membrane transport sites. Many bacterial pumps appear to be minimally affected by removal of their respective MBDs (Fan and Rosen, 2002; Mana-Capelli et al., 2003; Mandal and Arguello, 2003; Rice et al., 2006).

CopA is a Cu^+-dependent P_{IB} ATPase present in various bacteria, which typically has a single MBD in the N-terminal tail. CopA from *Archaeoglobus fulgidus* is unusual in having a second MBD on its C-terminal tail (Mandal et al., 2002); however, truncation or mutation of this C-terminal MBD does not have a significant affect on activity (Mandal and Arguello, 2003; Rice et al., 2006). In the present study, we have determined the structural location of the N-terminal MBD of CopA from *A. fulgidus* using cryoelectron microscopy to analyze tubular crystals of two different constructs. In particular, we have compared structures of a construct lacking the C-terminal MBD (ΔC-CopA) with another construct lacking both N- and C-terminal MBDs (ΔNΔC-CopA). Thus, we have identified the location of the N-terminal MBD relative to the N, P, and A domains that have been shown to drive catalysis. Difference maps show that the N-terminal MBD of CopA straddles the N domain and the A domain. By using the X-ray structure of Ca^{2+} ATPase as a template, we docked atomic coordinates corresponding to CopA cytoplasmic domains into our map and created a pseudoatomic model for the intact CopA molecule. This model reveals a conformational change in CopA that is consistent with the use of a phosphate analog (MgF_4^{2-}) for crystallization of ΔNΔC-CopA. In addition, the model suggests how the N-terminal MBD may be autoinhibitory in the Cu-free state, leading to a model for Cu-dependent regulation of CopA activity.

RESULTS

Crystallization of CopA

The two constructs of CopA used for crystallization are shown schematically in Figure 1 together with a polyacrylamide gel of the respective protein preparations. One construct produced a truncation of the C-terminal tail immediately after the last transmembrane helix (ΔC-CopA), whereas the other produced truncations of both N-terminal and C-terminal tails (ΔNΔC-CopA). Previous studies have documented that various constructs of CopA from *A. fulgidus*, including those studied here, require elevated temperatures for maximal levels of ATPase activity, an observation consistent with their derivation from the genome of an extreme thermophile (Mandal et al., 2002; Rice et al., 2006). Similarly, we found that elevated temperatures (~50°C) greatly favored the production of tubular crystals with helical symmetry. Although 2D arrays were also observed at room temperature, the proportion of tubular crystals was far lower. For ΔC-CopA, tubular crystals were grown in the presence of the Cu^+ chelator bathocuproindisulfonate (BCDS) at pH 6.1, which is analogous to the conditions used to stabilize the E_2 enzymatic state of SERCA1 (Takahashi et al., 2007; Toyoshima and Nomura, 2002). Tubular crystals of ΔNΔC-CopA grew under similar conditions with the addition of MgF_4^{2-}, a phosphate analog shown to stabilize the E_2-P state of SERCA1 (Toyoshima et al., 2004). In both cases, tubes were >10 μm long and narrow, with diameters of 30 nm and 35 nm for ΔC- and ΔNΔC-CopA, respectively (Figure 2).

Fourier transforms from tubular crystals preserved in the frozen hydrated state are characterized by a set of layer lines reflecting an underlying helical symmetry (Figure 2). Initially, these layer lines were assigned an arbitrary set of Miller indices and, ultimately, their helical selection rule was established by assigning a consistent set of Bessel orders (DeRosier and Moore, 1970). Similar to tubular crystals of SERCA1 and the nicotinic acetylcholine receptor, each construct of CopA produced a range of helical symmetries (Toyoshima and Unwin, 1990; Xu et al., 2002). For 3D reconstruction, we selected a group of tubes conforming to a single selection rule: for ΔC-CopA tubes, the (1,0) and (0,1) layer lines had Bessel orders of 5 and −8 respectively, whereas for ΔNΔC-CopA tubes, these primary layer lines had Bessel orders of 7 and −11. Although the axial positions of layer lines were variable, the corresponding changes in unit cell parameters were less than 2% (Table 1), indicating that Fourier-Bessel components of tubes within these respective symmetry groups could be averaged prior to 3D reconstruction. In the averaged data sets from ΔC-CopA and ΔNΔC-CopA tubes, the phase residuals were consistent with two-fold symmetry, which we therefore used to derive statistical measures of resolution. In particular, we used both two-fold related phase residuals and the Fourier shell correlation (FSC) after applying a 180° rotation to the unit cell. Table 1 indicates that averaged data from ΔC-CopA tubular crystals have slightly better resolution than ΔNΔC-CopA, which we judge to be ~17 Å.

Structure of CopA

Structures of ΔC-CopA and ΔNΔC-CopA are both characterized by a closely associated dimer (Figure 3 and Figure S1, see the Supplemental Data available with this article online). The

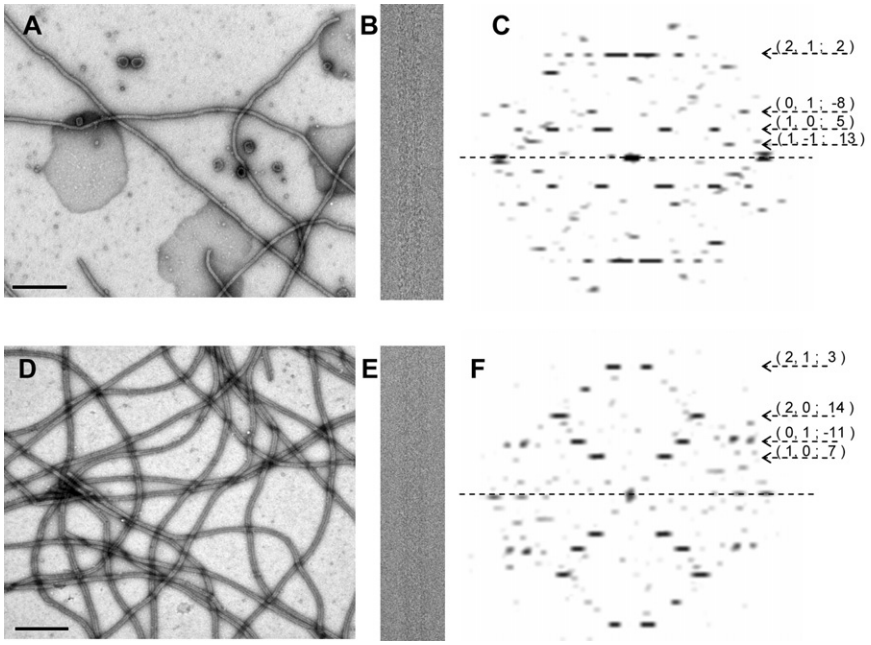

Figure 2. Tubular Crystals of CopA

(A–C) Raw data for ΔC-CopA with (A) low magnification of negatively stained samples, (B) higher magnification of an individual frozen-hydrated tube, and (C) its Fourier transform.

(D–F) Analogous data for ΔNΔC-CopA. Scale bar in negatively stained images corresponds to 0.5 μm. Numbers beside the Fourier transforms indicate the Miller indices of selected layer lines together with their assigned Bessel order, which are visible to ~25 Å.

physiological significance of this dimeric arrangement is uncertain because other members of the P-type ATPase family are known to be fully functional in the monomeric state (Jorgensen and Andersen, 1988). The boundaries of the bilayer were determined from the mean radial density distribution, which reveals two strong peaks arising from the electron-dense phosphates composing the lipid headgroups (Figure S2). The ΔC-CopA dimer (Figures 3A–3C) fits within a cylinder 76 Å in diameter and 108 Å long. The cytoplasmic domains extend ~78 Å above the bilayer surface, whereas the extracellular domains are not resolved from the inner leaflet of the bilayer. The shape of the cytoplasmic domains is generally reminiscent of Na^+,K^+ ATPase (Rice et al., 2001) and Ca^{2+} ATPase (Zhang et al., 1998) in the E_2 conformation. The cytoplasmic headpiece of all three molecules is pear shaped, though in the side view of ΔC-CopA (Figure 3B) there is a low-density hole appearing at the center of the cytoplasmic domains. A similar, though smaller, hole was previously seen in Ca^{2+} ATPase that had been labeled by FITC prior to crystallization (Xu et al., 2002). Although the dimensions of the ΔNΔC-CopA dimer are similar, the cytoplasmic domains are more closely associated, thus filling this hole and reducing the length of the pear-shaped cytoplasmic headpiece (Figures 3D–3F).

Table 1. Statistics of Data Averaging

		ΔC-CopA	ΔNΔC-CopA
N (1,0)		5	7
N (0,1)		−8	−11
No. of tubes		11	13
No. of dimers		2397	5873
Unit cell dimensions	a (Å)	75 ± 1.1	71.2 ± 1.5
	b (Å)	47 ± 0.7	47.4 ± 0.7
	γ (°)	69.9 ± 0.8	65.9 ± 0.9
Two-fold phase residual[a]	∞–35 Å (°)	7.9	6.5
	35–25 Å (°)	10.4	10.0
	25–20 Å (°)	29.5	31.3
	20–17.5 Å (°)	39.0	38.9
	17.5–15 Å (°)	40.2	41.6
FSC[b]	0.5 (Å)	17.3	17.5
	0.3 (Å)	14.8	15.9

[a] Phase residual in the indicated resolution bins.

[b] Resolution at which the Fourier shell coefficient falls to the indicated value.

Model for CopA

Our goal was to use these structures to build a pseudoatomic model for CopA and thus to define the location of the N-terminal MBD. As a first step, we calculated a difference map between the cytoplasmic domains of ΔC-CopA and ΔNΔC-CopA. When plotted at 2.5σ, this difference map revealed three positive densities, labeled D1, D2, and D3 (Figures 4A–4C), and one negative density occupying the hole in the middle of the headpiece (Figures 4G–4I). Next, we fit atomic models derived from X-ray crystal structures of isolated CopA cytoplasmic domains to the maps (Figures 4D–4F). To guide this fit, X-ray structures for the isolated N-/P-domain pair (Sazinsky et al., 2006b) and for the isolated A domain (Sazinsky et al., 2006a) were aligned with a structure of Ca^{2+}-ATPase in the analogous E_2 conformation (Takahashi et al., 2007). After this alignment, these three cytoplasmic domains were then fitted as a rigid body into the cytoplasmic region of our ΔC-CopA (Figure S3). To optimize this fit, the N domain was rotated slightly (<10°) away from the A domain to produce the structure shown in Figures 4D–4F. A similar procedure was used for fitting ΔNΔC-CopA, except that the structure of Ca^{2+}-ATPase in the E_2-P conformation (Toyoshima et al., 2004) was used as a template for rigid-body docking and, in this case, the N domain was rotated ~10° toward the A domain (Figure S3). These small adjustments to the N domain are consistent with the demonstrated flexiblility of the loops connecting it to the P domain and with the wide variety of angles observed in structures of Ca^{2+} ATPase (Kuhlbrandt, 2004; Toyoshima and Inesi, 2004). Although we attempted automated docking of these domains using the program Chimera (Pettersen et al., 2004), it produced a nonphysiological rotation of the N-/P-domain pair relative to the A domain.

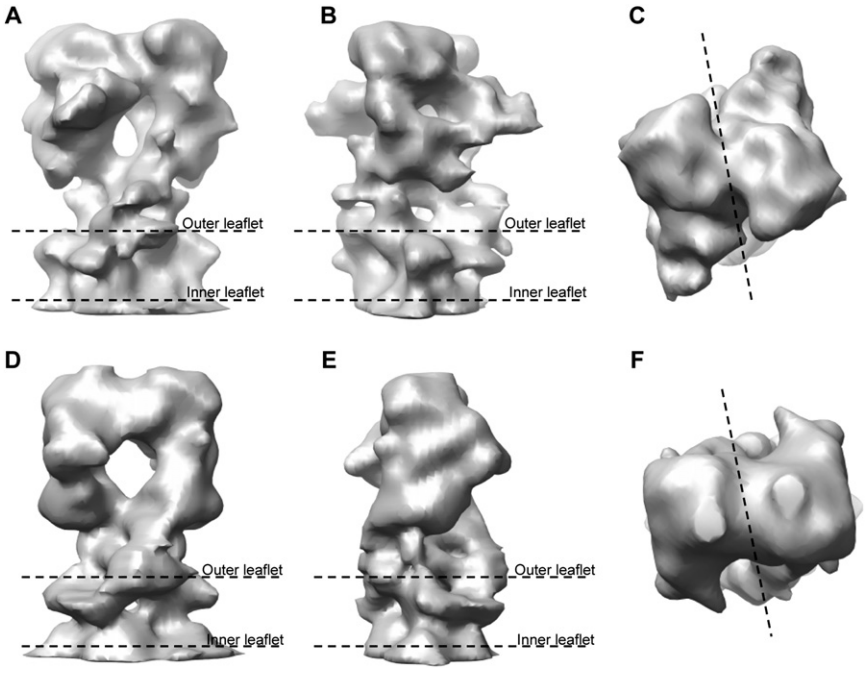

Figure 3. 3D Reconstruction of CopA

(A–C) Orthogonal views of the ΔC-CopA dimer that composes the unit cell.

(D–F) Analogous views of the ΔNΔC-CopA dimer. The boundary of the membrane is indicated in side views with "outer leaflet" referring to the outer surface of the tube (Figure S1). The dotted line in (C) and (F) shows the boundary between the monomers.

In light of these atomic models, the difference densities labeled D2 and D3 in Figure 4 are consistent with a conformational change in the N domain, caused by its movement relative to the A domain. This movement also contributes to the hole observed in the middle of the ΔC-CopA cytoplasmic headpiece and the corresponding negative difference density in that location. However, this conformational change fails to account for the larger difference density D1, which we believe to reflect the presence of the N-terminal MBD in ΔC-CopA but not in ΔNΔC-CopA. Unoccupied density is present in this region of the ΔC-CopA map (Figures 4D–4F) but not in the density map of ΔNΔC-CopA (Figures 5G–5I). To explore the plausibility of this assignment, we docked the X-ray structure for the N-terminal MBD from *Bacillus subtilis* CopA (Banci et al., 2002a) next to the A domain of ΔC-CopA. Orientation of the C terminus of this MBD toward the transmembrane represented an important constraint for this docking, though the shape of the MBD largely dictated its final orientation (Figure 5).

The transmembrane region in our maps was consistent with the presence of eight transmembrane helices, as predicted for CopA. Sequence analysis of of P_{IB} ATPases suggests that six of these helices correspond to the first six transmembrane helices of P_{II} ATPases, and that two additional helices have been added to the N-terminal end of the molecule (Lutsenko and Kaplan, 1995). Thus, we built the transmembrane portion of our CopA model by placing the first six transmembrane helices of Ca^{2+} ATPase in locations dictated by an alignment of P domains. Overall, these six helices fit well within the transmembrane density of CopA, but left empty density within the transmembrane envelope. We were then able to fit two additional helices within this envelope near the Ca^{2+} ATPase M1 helix. Based on sequence alignments, these extra two helices were initially assigned as M1-M2, but a recent study of CopA proteolysis suggests that they might instead follow the first transmembrane helix of P_{II} pumps, making them M2-M3 (Hatori et al., 2007; Figure 1). We have assigned these additional helices as M2 and M3 in Figure 6, which shows the fit at two different sections through the membrane for both CopA constructs.

DISCUSSION

We have presented structures of two CopA constructs at 17 Å resolution, which we have used as templates for constructing pseudoatomic models. The structures differ in two respects—namely, the ligands used for crystallization and the presence of the N-terminal MBD. Comparison of these two structures suggests that the N-terminal MBD is located within the cytoplasmic head and further suggests that CopA undergoes a conformational change that may be related to the presence of a phosphate analog at the catalytic site.

Based on the modeling of our two structures, the N-terminal MBD of CopA appears to lie between the N and A domains (Figure 7), which are conserved cytoplasmic domains found in all P-type ATPases. Although MBDs are unique to the P_{IB} subfamily, a small N-terminal domain precedes the first transmembrane helix of other P-type ATPases and generally consists of a pair of α helices. In the X-ray structures of Ca^{2+} ATPase (Toyoshima et al., 2000), Na^+/K^+ ATPase (Morth et al., 2007), and H^+ ATPase (Pedersen et al., 2007), this pair of α helices binds to the distal part of the β-barrel that constitutes the A domain (e.g., Figure S3E). A 10- to 15-residue unstructured loop connects these two α helices to M1. This N-terminal domain forms an integral part of the A domain and does not become displaced during the various conformational changes that accompany the catalytic cycle of Ca^{2+} ATPase. Flexibility in the unstructured loop is essential for the dramatic movements of the A domain during this cycle. However, the tugging of this loop on M1 is thought to initiate closing of the cytoplasmic ion gate upon formation of the high-energy phosphoenzyme (E1∼P) (Sorensen et al., 2004; Toyoshima and Mizutani, 2004). A recent proteolysis study of CopA from *T. maritima* suggested that its N-terminal MBD also formed an integral part of the A domain and that the first transmembrane helix was analogous to the bent M1 helix seen in structures of Ca^{2+} ATPase, Na^+/K^+ ATPase, and H^+ ATPase (Hatori et al., 2007). This study also concluded that the two extra transmembrane helices at the N terminus of CopA are inserted between M1 and M2 of Ca^{2+} ATPase. Our structural analysis of CopA from *A. fulgidus* is consistent with these hypotheses, though the binding site of the N-terminal MBD on the A domain

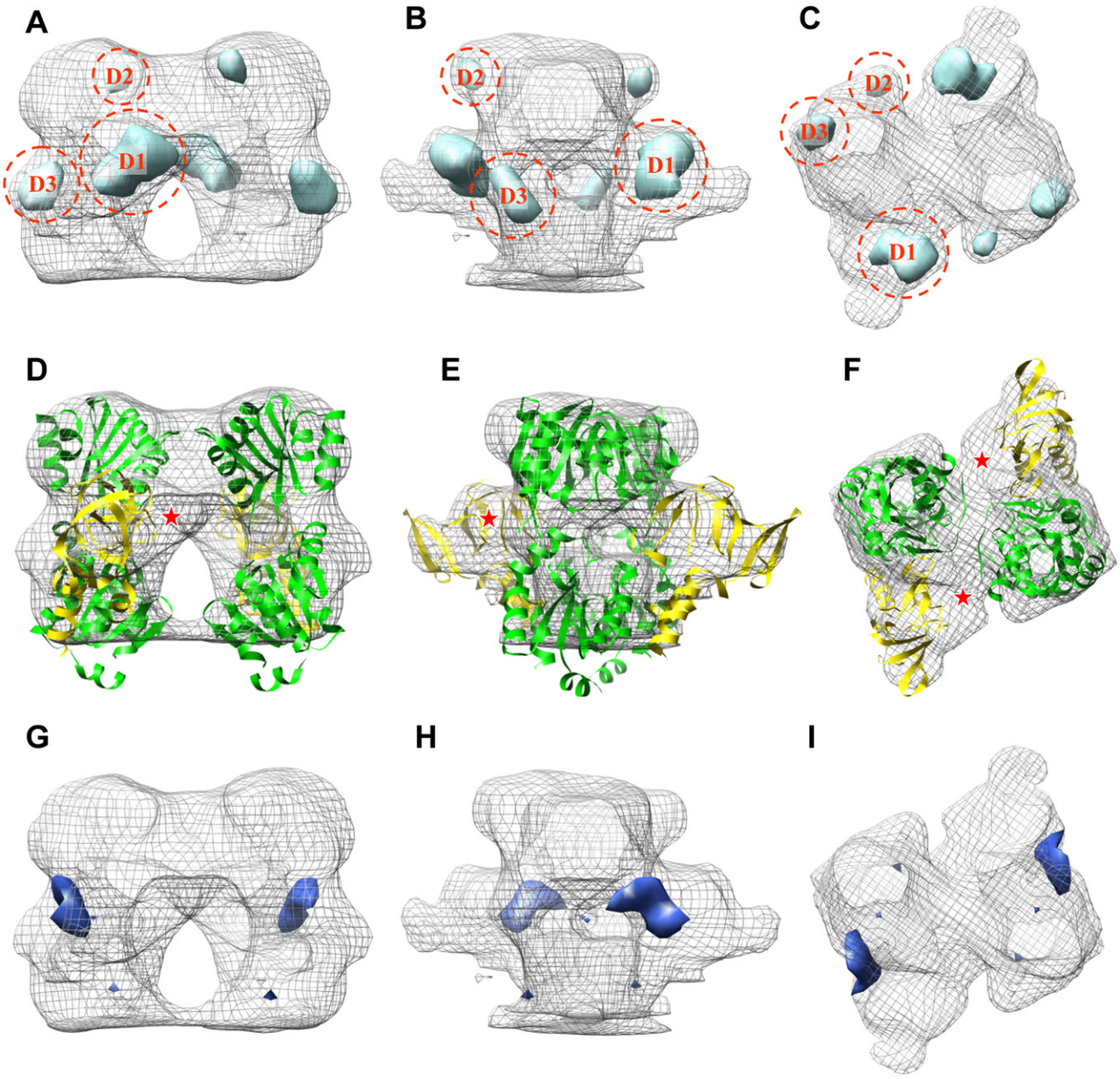

Figure 4. Difference Map for ΔC-CopA Minus ΔNΔC-CopA

(A–C) Positive difference densities (light blue) plotted at 2.5σ superimposed on the envelope of ΔC-CopA (gray mesh).

(D–F) Fitting of cytoplasmic domains to the envelope of ΔC-CopA, revealing an unoccupied region that likely corresponds to the N-terminal MBD (red asterisk).

(G–I) A single negative-difference density at 2.5σ from the difference map (dark blue). Views are as in Figure 3.

is markedly different from the two N-terminal helices of the other P-type ATPases. Our sequence alignments indicate that there are ~11 residues between the last β strand of the N-terminal MBD from *A. fulgidus* CopA and the bent M1 helix (Figure S4), which if extended could readily span the corresponding distance in our model. The putative locations of M2 and M3 in our model could also be reached by this linker; therefore, this plausible assignment for M1 must remain tentative.

Although the resolution of our map is low, the envelope constrains the location of the N-terminal MBD relative to the other cytoplasmic domains to a considerably higher degree. The legitimacy of this modeling approach has been demonstrated for Ca^{2+} ATPase (Xu et al., 2002) and Na^{+}/K^{+} ATPase (Rice et al., 2001), for which pseudoatomic models created in a similar fashion were subsequently confirmed by X-ray crystallographic structures. The βαββαβ fold of MBDs consists of two α helices packed against a four-stranded β sheet and fits nicely within unoccupied density between the N and A domains (Figures 4 and 5). The Cu-binding GMTCxxC motif lies in the loop following the first α helix, which caps a hydrophobic core between the

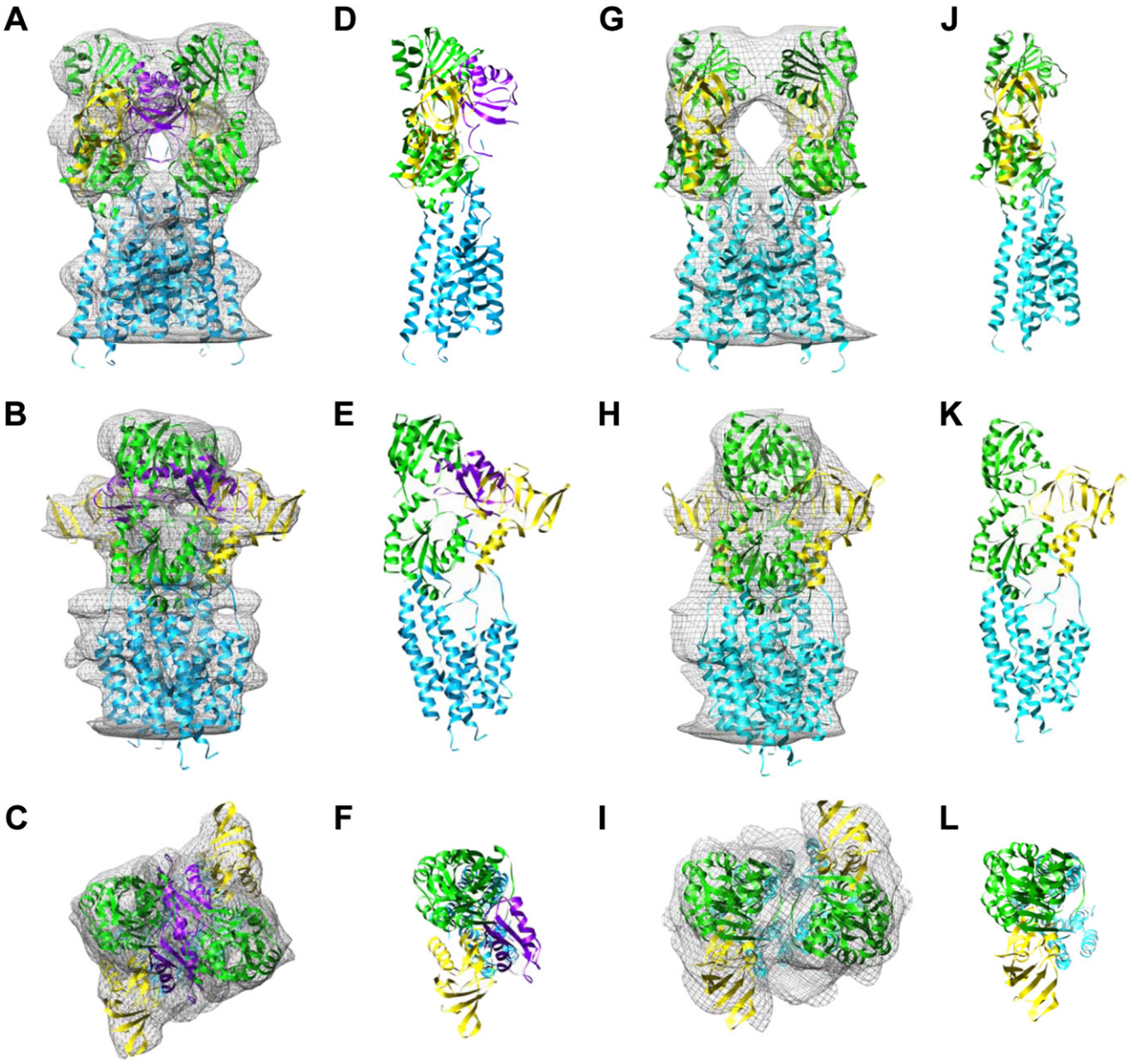

Figure 5. Atomic Model for CopA Docked to the Maps
(A–F) Model for ΔC-CopA.
(G–L) Model for ΔNΔC-CopA.
Domains colored as follows: transmembrane helices (cyan), P/N domain (green), A domain (yellow), N-terminal MBD (magenta).

sheet and the helices. According to our fit, the side of the N-terminal MBD packs against the side of the A domain, and the Cu-binding GMTCxxC loop interacts with the N domain (Figure 7). The site of this N domain interaction involves the ERRSEHP^{463} loop, which is highly homologous in MNK and WNDP pumps, where it has been implicated in ATP binding (Dmitriev et al., 2006; Morgan et al., 2004). The α-helical surface of the MBD is solvent exposed, which would potentially allow for its interaction with metallochaperones. Charged residues on this surface have been implicated in mediating the interaction and defining the specificity of MBD with its corresponding metallochaperone (Arnesano et al., 2002, 2004; Wernimont et al., 2000).

Previous work on P_{IB} ATPases has proposed two different roles for the MBDs. The human MNK and WNDP pumps have six tandem MBDs (MBD1–6). The first four appear to regulate activity by modifying the binding of ATP to the pump in a Cu-dependent manner (Huster and Lutsenko, 2003). Specifically, direct binding has been shown between the N-terminal MBDs and the ATP-binding domain of WNDP in a way that suggests autoinhibitory behavior of these MDBs in the absence of Cu and relief from this inhibition in the presence of Cu (Tsivkovskii et al., 2001).

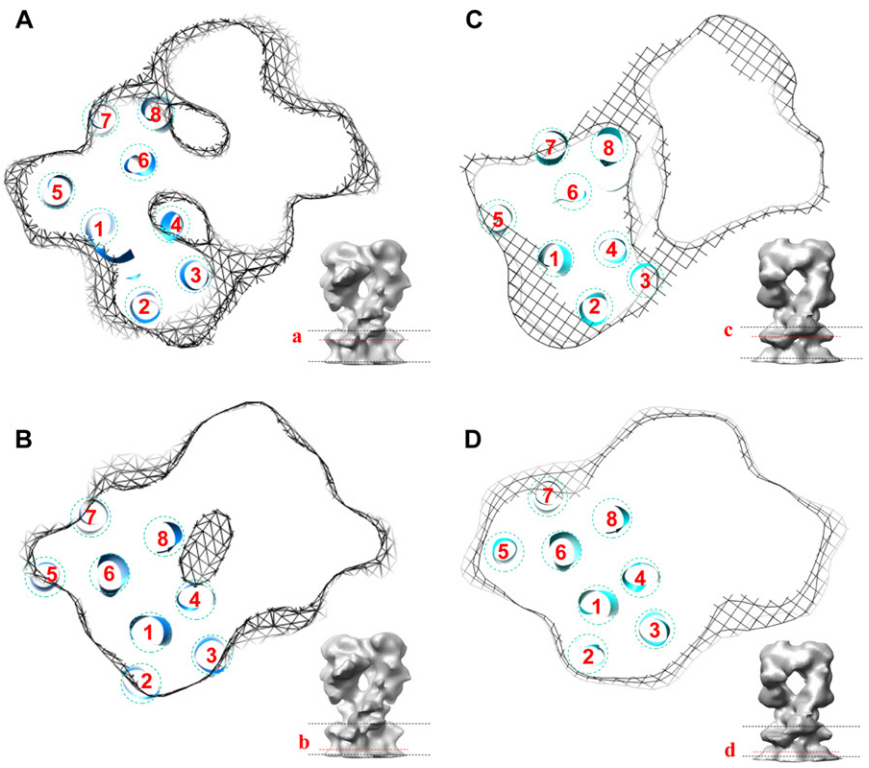

Figure 6. Location of the Transmembrane Helices of CopA

(A and B) Helices fitted to one monomer of the ΔC-CopA dimer in two sections near the (A) top and (B) bottom of the membrane.

(C and D) ΔNΔC-CopA helices at similar locations in the membrane, indicated in the inset to each panel. The arrangement of helices and their location relative to the P domain was the same in both models; slight differences in appearance reflect a different depth of the respective sections within the membrane.

In contrast, mutations to MBD5 or 6 alter the apparent affinity of the intramembrane Cu transport sites (Huster and Lutsenko, 2003), though the mechanism for this effect is unclear. Cu transfer has been demonstrated from the metallochaperone Atox1 to MBD1–4 and also from MBD4 to MBD5,6 (Achila et al., 2006) and can be explained by a sequential exchange of cysteine ligands at the exposed Cu-binding sites (Wernimont et al., 2000). However, the transport sites are buried within a group of packed transmembrane helices, and it is hard to envision how direct transfer from an MBD could be accomplished. Furthermore, all the bacterial P_{IB} ATPases appear functional in the absence of their N-terminal MBDs (Bal et al., 2001; Fan and Rosen, 2002; Mana-Capelli et al., 2003; Mandal and Arguello, 2003; Mitra and Sharma, 2001; Rice et al., 2006), suggesting that the more likely explanation is that Cu binding to these MBDs exerts an allosteric effect on global protein conformation, thus facilitating Cu binding to the transport sites.

Considering this work in the context of our CopA structure leads us to propose the following model. Like other P-type ATPases, the N-terminal MBD appears to be an integral part of the A domain. In the Cu-free state, the MBD interacts with the N domain and either prevents ATP binding or prevents the domain movement necessary to transfer the γ-phosphate to the catalytic aspartate, thus producing an autoinhibited state. Recognition of the MBD by Cu-loaded metallochaperone disrupts this interaction and leads to transfer of Cu to the MBD. Once loaded with Cu, the MBD is no longer able to interact with the N domain, thus allowing ATP binding, transfer of γ-phosphate, and subsequent steps for Cu transport. This could explain the observation of substantially reduced activity of CopA caused by mutations in the CxxC motif that presumably prevent binding of Cu to the N-terminal MBD (Mandal and Arguello, 2003). It is not yet clear from our work whether the MBD remains associated with the A domain in the Cu-bound state or is able to swing down and dock at some location next to the membrane to deliver its Cu to the transport sites.

We used different conditions for crystallization of our two CopA constructs, which can be expected to induce different intermediates in the reaction cycle. In particular, ΔC-CopA was crystallized in the presence of Cu chelator (BCDS), whereas ΔNΔC-CopA required the addition of the phosphate analog MgF_4^{2-} in addition to this chelator. These conditions were chosen empirically to optimize crystallization, but they also allow us to evaluate potential conformational changes of CopA that accompany the transition between the respective reaction intermediates. In the case of Ca^{2+} ATPase, X-ray crystal structures have been reported for the analogous intermediates, termed E2 for the chelator (EGTA) alone (Takahashi et al., 2007; Toyoshima and Nomura, 2002) and E2-P upon the addition of MgF_4^{2-} (Toyoshima et al., 2004). Although the membrane domains of the two structures are comparable, there are distinct differences in the cytoplasmic domains caused by the presence of the phosphate analog. Specifically, the A and P domains are more tightly packed in the E2-P conformation because of the role the conserved TGES loop plays within the A domain in orienting a water molecule for hydrolysis of the aspartyl phosphate in the P domain. In the absence of phosphate, there are no specific ligands holding the A domain close to the catalytic site, allowing the two domains to move apart (Moller et al., 2005; Toyoshima and Inesi, 2004). Comparison of our CopA structures reveals a similar structural difference, with the cytoplasmic domains of ΔNΔC-CopA in the presence of MgF_4^{2-} being tightly packed, whereas the structure ΔC-CopA actually has a low-density hole separating the A and P domains. The presence of the MBD in the latter structure is also likely to influence the domain interactions and, in the latter case, to pry the A domain away from the N and P domains. MgF_4^{2-} substantially improved crystal order of ΔNΔC-CopA, suggesting that its ability to stabilize the A-/P-domain interface was an important factor. In contrast, MgF_4^{2-} interfered with crystallization of ΔC-CopA, implying a competition between MgF_4^{2-} binding and the MBD-stabilized state. Such a competition is consistent with our proposed

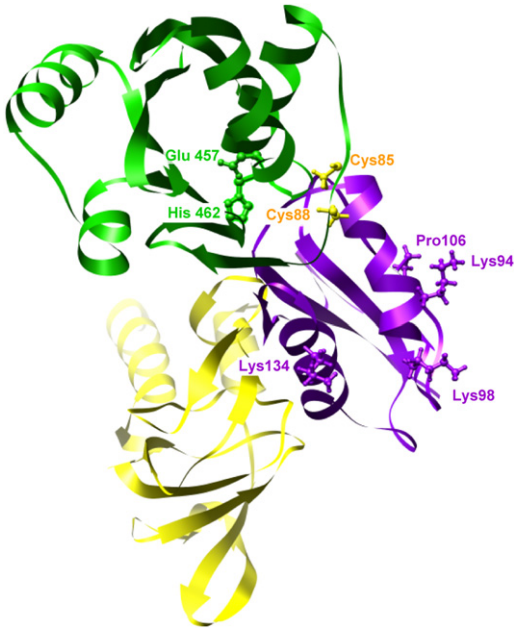

Figure 7. Interactions between the Cytoplasmic Domains
The N-terminal MBD (magenta) is shown interacting with the A domain (yellow) and the ATP-binding N domain (green). Several residues from the MBD implicated in recognizing the metallochaperone are shown in ball-and-stick representation in magenta, and the conserved, metal-liganding cysteine residues from the MBD are shown in ball-and-stick representation in yellow (sequence numbers correspond to *B. subtilis*). The conserved Glu and His from an ATP-binding loop of the CopA N domain are also shown in ball-and-stick representation in green, near the site of interaction with the MBD (sequence numbers correspond to *A. fulgidus*). This view is similar to Figure 5F.

role for the Cu-free MBD in preventing the necessary domain interaction and thus promoting an autoinhibited state.

EXPERIMENTAL PROCEDURES

CopA Constructs

Two CopA constructs were used for crystallization (Figure 1). The first involved truncation of 68 residues from the C terminus (ΔC-CopA) and the other involved a double truncation of the C terminus together with 95 residues from the N terminus (ΔNΔC-CopA). These truncations were designed to interrupt the native protein immediately adjacent to the respective transmembrane helix. Expression plasmids (pBAD) containing CopA constructs with histidine tags were obtained as described previously (Rice et al., 2006).

Protein Expression and Purification

E. coli (LMG1940) transformed with plasmids containing CopA constructs was cultured in LB broth with 0.1 mg/ml ampicillin at 37°C. After growing to an OD of 1, expression was induced with 0.02% arabinose for 2 hr at 30°C before harvesting cells by centrifugation at 10,000 × g for 10 min at 4°C. The pellet was suspended in a buffer composed of 50 mM Tris-Cl (pH 7.5), 20% glycerol, 50 mM NaCl, 2 mM β-mercaptoethanol, 0.05 mg/ml DNase I, and complete protease inhibitor cocktail (Roche, Basel, Switzerland) according to manufacturer's instructions. Cell membranes were broken by French Press at 20,000 psi, and debris was removed by centrifugation at 12,000 × g for 20 min at 4°C. Membranes were then collected by centrifugation at 150,000 × g for 1h at 4°C and stored at −80°C.

Membrane pellets were resuspended in a standard buffer (25 mM Tris-Cl [pH 7.5], 100 mM NaCl, 10% glycerol, 2 mM β-mercaptoethanol) with 20 mM imidazole, EDTA-free protease inhibitor cocktail and 10 mg/ml dodecylmaltoside (DDM) at a total protein concentration of 10 mg/ml. After gently mixing for 30 min at 4°C, insoluble material was removed by centrifugation at 150,000 × g for 30 min at 4°C. The protein supernatant was then loaded onto a 5 ml HiTrap Chelating HP column (GE Healthcare), which was charged previously with 0.1 M $NiCl_2$ and equilibrated with standard buffer supplemented with 20 mM imidazole and 0.1% DDM. After washing, purified CopA protein was eluted with standard buffer supplemented with 400 mM imidazole and 0.1% DDM. The His-tag was removed from CopA by overnight incubation with 1 U thrombin per milligram of protein at 4°C. Thrombin was then removed with a benzamidine-Sepharose column (Amersham Biosciences) equilibrated with standard buffer with 0.1% DDM. Finally, CopA was dialyzed against 25 mM Tris-Cl (pH 7.5), 100 mM Na_2SO_4, 10% glycerol, 2 mM DTT, and 0.1% DDM. Protein concentration was determined by absorbance at 280 nm. This procedure typically produced 5–8 mg of purified protein from 6 l of bacterial media. SDS-PAGE showed that the samples were >95% pure and thus suitable for crystallization trials (Figure 1).

Crystallization and Electron Microscopy

Tubular crystals of ΔC-CopA were grown by adding dioleoylphosphatidylcholine (0.4 mg/mg protein) and dialyzing the resulting protein mixture (0.5 mg/ml total protein in 50 μl dialysis button) against 50 mM MES (pH 6.1), 25 mM Na_2SO_4, 25 mM K_2SO_4, 200 μM BCDS, 10 mM $MgSO_4$, and 2 mM β-mercaptoethanol for 5 days at 45°C–55°C. Tubular crystals of ΔNΔC-CopA were grown under similar conditions except that 1 mM NaF was added to the dialysis buffer. For electron microscopy, a suspension of crystals was deposited on a holey carbon grid and rapidly frozen in liquid ethane. Samples were imaged at −175°C with a CT3500 cryoholder (Gatan UK) at 50,000× magnification with a CM200 FEG electron microscope (FEI Corp.) operating at 200 kV. Defocus values ranged from 9,000 to 25,000 Å. Electron micrographs were recorded on film and, after screening by optical diffraction, suitable images were digitized at 14 μm intervals with a Zeiss SCAI microdensitometer (Intergraph Corp.).

Image Analysis

Helical reconstruction was carried out as previously described (Stokes et al., 2005; Xu et al., 2002). The helical symmetry was determined by assigning Bessel orders to principal layer lines labeled as (1,0) and (0,1) in Figure 2. The initial assignment was based on the expected location of the first maximum of the corresponding Bessel function $J_n(2\pi Rr)$, where n is the Bessel order, R is the observed distance of the first maximum along the layer line from the meridian, and r is the radius of the tube in real space. These initial assignments were checked in several ways. First, the phases of peaks across the low-lying layer lines should be equal for even Bessel orders or differ by 180° for odd Bessel orders. Second, the Bessel orders for other layer lines could be predicted from the principal layer lines, and the distance of their initial peaks from the meridian should be consistent with these predictions. Finally, the determination of out-of-plane tilt is sensitive to these Bessel-order assignments, and the correct indexing scheme inevitably produced the lowest phase residual after applying the corresponding corrections (DeRosier and Moore, 1970). Handedness of the helical lattice was determined by tilting samples ~30° about an axis normal to the long axis of the tubes and analyzing the diffraction patterns from the left half and right half of the resulting images (Finch, 1972). Thus, the layer line designated as 1,0 (Figure 2) was determined to be right-handed. Several helical symmetry groups were found for ΔC-CopA and ΔNΔC-CopA tubes (Toyoshima and Unwin, 1990), but only those with the selection rules shown in Figure 2 were used for further analysis. Each of these data sets was analyzed by the methods of Beroukhim and Unwin (1997). Correction for the contrast transfer function was based on an amplitude contrast of 7% (Toyoshima et al., 1993). For the final maps, a Butterworth filter was applied using SPIDER (Frank et al., 1996) with passband and stopband frequency of 13.3 Å and 9.5 Å, respectively.

For calculation of a difference map, the cytoplasmic domains of the two maps were isolated, and an isodensity contour was chosen to provide the expected volume for ΔC-CopA, assuming the value of 1.21 $Å^3$ per dalton (Harpaz et al., 1994). The density values for ΔNΔC-CopA were then scaled such that the same isodensity contour gave the expected volume, taking into account the missing N-terminal MBD. After scaling, the dimer was masked from each map and aligned, and a simple subtraction was performed using SPIDER.

Docking of Atomic Coordinates

An initial model for CopA was created by superimposing atomic coordinates of N-/P-domain pair (2B8E) (Sazinsky et al., 2006b) and the A domain (2HC8) (Sazinsky et al., 2006a) onto the X-ray crystallographic structure of Ca^{2+} ATPase in either the E2 (2EAR) (Takahashi et al., 2007) or E2-MgF_4^{2-} (1WPG) (Toyoshima et al., 2004) conformation (Figure S3) using the MatchMaker routine in Chimera (Pettersen et al., 2004). The transmembrane domain was initially modeled as the first six helices from Ca^{2+} ATPase. The resulting CopA models were then docked manually into the density maps. To optimize the fit, the N domain and A domain were adjusted slightly to match the map density and two additional helices, derived from Ca^{2+} ATPase M7 and M10, were placed into the transmembrane domain. Finally, the N-terminal MBD from *B. subtilis* (1JWW) (Banci et al., 2002a) was placed into the map to occupy unassigned density in the cytoplasmic headpiece. The model was initially fitted to a monomer of CopA, whose boundaries were evident from the map (see Figure 3). The model was then duplicated and manually manipulated to fit into the two-fold related symmetry partner. No significant steric clashes resulted from placing this second molecule within the dimeric density, providing added confidence in the fit.

ACCESSION NUMBERS

The maps have been deposited in the EM Data Bank under accession numbers EMD-5004 and EMD-5005, and the corresponding atomic models have been deposited in the Protein Data Bank under accession number 2VOY.

SUPPLEMENTAL DATA

Supplemental Data include four figures and can be found with this article online at http://www.structure.org/cgi/content/full/16/6/976/DC1/.

ACKNOWLEDGMENTS

The authors acknowledge Aleksandra Kovalishin for early work in expression and purification of CopA. This research utilized the facilities at the New York Structural Biology Center (a STAR center supported by the New York State Office of Science, Technology, and Academic Research) and was supported by NIH grant GM56960 to D.L.S.

Received: January 7, 2008
Revised: February 18, 2008
Accepted: February 19, 2008
Published: June 10, 2008

REFERENCES

Achila, D., Banci, L., Bertini, I., Bunce, J., Ciofi-Baffoni, S., and Huffman, D.L. (2006). Structure of human Wilson protein domains 5 and 6 and their interplay with domain 4 and the copper chaperone HAH1 in copper uptake. Proc. Natl. Acad. Sci. USA *103*, 5729–5734.

Arguello, J.M., Eren, E., and Gonzalez-Guerrero, M. (2007). The structure and function of heavy metal transport P1B-ATPases. Biometals *20*, 233–248.

Arnesano, F., Banci, L., Bertini, I., Ciofi-Baffoni, S., Molteni, E., Huffman, D.L., and O'Halloran, T.V. (2002). Metallochaperones and metal-transporting ATPases: a comparative analysis of sequences and structures. Genome Res. *12*, 255–271.

Arnesano, F., Banci, L., Bertini, I., and Bonvin, A.M. (2004). A docking approach to the study of copper trafficking proteins; interaction between metallochaperones and soluble domains of copper ATPases. Structure *12*, 669–676.

Axelsen, K.B., and Palmgren, M.G. (1998). Evolution of substrate specificities in the P-type ATPase superfamily. J. Mol. Evol. *46*, 84–101.

Bal, N., Mintz, E., Guillain, F., and Catty, P. (2001). A possible regulatory role for the metal-binding domain of CadA, the *Listeria* monocytogenes Cd^{2+}-ATPase. FEBS Lett. *506*, 249–252.

Banci, L., Bertini, I., Ciofi-Baffoni, S., D'Onofrio, M., Gonnelli, L., Marhuenda-Egea, F.C., and Ruiz-Duenas, F.J. (2002a). Solution structure of the N-terminal domain of a potential copper-translocating P-type ATPase from *Bacillus subtilis* in the apo and Cu(I) loaded states. J. Mol. Biol. *317*, 415–429.

Banci, L., Bertini, I., Ciofi-Baffoni, S., Finney, L.A., Outten, C.E., and O'Halloran, T.V. (2002b). A new zinc-protein coordination site in intracellular metal trafficking: solution structure of the Apo and Zn(II) forms of ZntA(46–118). J. Mol. Biol. *323*, 883–897.

Banci, L., Bertini, I., Del Conte, R., D'Onofrio, M., and Rosato, A. (2004). Solution structure and backbone dynamics of the Cu(I) and apo forms of the second metal-binding domain of the Menkes protein ATP7A. Biochemistry *43*, 3396–3403.

Beroukhim, R., and Unwin, N. (1997). Distortion correction of tubular crystals: Improvements in the acetylcholine receptor structure. Ultramicroscopy *70*, 57–81.

DeRosier, D.J., and Moore, P.B. (1970). Reconstruction of three-dimensional images from electron micrographs of structures with helical symmetry. J. Mol. Biol. *52*, 355–369.

DiDonato, M., and Sarkar, B. (1997). Copper transport and its alterations in Menkes and Wilson diseases. Biochim. Biophys. Acta *1360*, 3–16.

Dmitriev, O., Tsivkovskii, R., Abildgaard, F., Morgan, C.T., Markley, J.L., and Lutsenko, S. (2006). Solution structure of the N-domain of Wilson disease protein: distinct nucleotide-binding environment and effects of disease mutations. Proc. Natl. Acad. Sci. U.S.A. *103*, 5302–5307.

Fan, B., and Rosen, B.P. (2002). Biochemical characterization of CopA, the *Escherichia coli* Cu(I)-translocating P-type ATPase. J. Biol. Chem. *277*, 46987–46992.

Finch, J.T. (1972). The hand of the helix of tobacco virus. J. Mol. Biol. *66*, 291–294.

Forbes, J.R., Hsi, G., and Cox, D.W. (1999). Role of the copper-binding domain in the copper transport function of ATP7B, the P-type ATPase defective in Wilson disease. J. Biol. Chem. *274*, 12408–12413.

Frank, J., Radermacher, M., Penczek, P., Zhu, J., Li, Y., Ladjadj, M., and Leith, A. (1996). SPIDER and WEB: processing and visualization of images in 3D electron microscopy and related fields. J. Struct. Biol. *116*, 190–199.

Gitschier, J., Moffat, B., Reilly, D., Wood, W.I., and Fairbrother, W.J. (1998). Solution structure of the fourth metal-binding domain from the Menkes copper-transporting ATPase. Nat. Struct. Biol. *5*, 47–54.

Harpaz, Y., Gerstein, M., and Chothia, C. (1994). Volume changes on protein folding. Structure *2*, 641–649.

Hatori, Y., Majima, E., Tsuda, T., and Toyoshima, C. (2007). Domain organization and movements in heavy metal ion pumps: papain digestion of CopA, a Cu+-transporting ATPase. J. Biol. Chem. *282*, 25213–25221.

Haupt, M., Bramkamp, M., Coles, M., Altendorf, K., and Kessler, H. (2004). Inter-domain motions of the N-domain of the KdpFABC complex, a P-type ATPase, are not driven by ATP-induced conformational changes. J. Mol. Biol. *342*, 1547–1558.

Huster, D., and Lutsenko, S. (2003). The distinct roles of the N-terminal copper-binding sites in regulation of catalytic activity of the Wilson's disease protein. J. Biol. Chem. *278*, 32212–32218.

Jorgensen, P.L., and Andersen, J.P. (1988). Structural basis for E_1-E_2 conformational transitions in Na,K-pump and Ca-pump proteins. J. Membr. Biol. *103*, 95–120.

Kuhlbrandt, W. (2004). Biology, structure and mechanism of P-type ATPases. Nat. Rev. Mol. Cell Biol. *5*, 282–295.

Lee, S., Kim, Y.Y., Lee, Y., and An, G. (2007). Rice P1B-type heavy-metal ATPase, OsHMA9, is a metal efflux protein. Plant Physiol. *145*, 831–842.

Lubben, M., Guldenhaupt, J., Zoltner, M., Deigweiher, K., Haebel, P., Urbanke, C., and Scheidig, A.J. (2007). Sulfate acts as phosphate analog on the monomeric catalytic fragment of the CPx-ATPase CopB from *Sulfolobus solfataricus*. J. Mol. Biol. *369*, 368–385.

Lutsenko, S., and Kaplan, J.H. (1995). Organization of P-type ATPases: significance of structural diversity. Biochemistry *34*, 15607–15613.

Lutsenko, S., Barnes, N.L., Bartee, M.Y., and Dmitriev, O.Y. (2007). Function and regulation of human copper-transporting ATPases. Physiol. Rev. *87*, 1011–1046.

Mana-Capelli, S., Mandal, A.K., and Arguello, J.M. (2003). *Archaeoglobus fulgidus* CopB is a thermophilic Cu^{2+}-ATPase: functional role of its histidine-rich-N-terminal metal binding domain. J. Biol. Chem. *278*, 40534–40541.

Mandal, A.K., and Arguello, J.M. (2003). Functional roles of metal binding domains of the *Archaeoglobus fulgidus* Cu^{+}-ATPase CopA. Biochemistry *42*, 11040–11047.

Mandal, A.K., Cheung, W.D., and Arguello, J.M. (2002). Characterization of a thermophilic P-type Ag^{+}/Cu^{+}-ATPase from the extremophile *Archaeoglobus fulgidus*. J. Biol. Chem. *277*, 7201–7208.

Mitra, B., and Sharma, R. (2001). The cysteine-rich amino-terminal domain of ZntA, a Pb(II)/Zn(II)/Cd(II)-translocating ATPase from *Escherichia coli*, is not essential for its function. Biochemistry *40*, 7694–7699.

Moller, J.V., Juul, B., and le Maire, M. (1996). Structural organization, ion transport, and energy transduction of P-type ATPases. Biochim. Biophys. Acta *1286*, 1–51.

Moller, J.V., Olesen, C., Jensen, A.M., and Nissen, P. (2005). The structural basis for coupling of Ca^{2+} transport to ATP hydrolysis by the sarcoplasmic reticulum Ca^{2+}-ATPase. J. Bioenerg. Biomembr. *37*, 359–364.

Morgan, C.T., Tsivkovskii, R., Kosinsky, Y.A., Efremov, R.G., and Lutsenko, S. (2004). The distinct functional properties of the nucleotide-binding domain of ATP7B, the human copper-transporting ATPase: analysis of the Wilson disease mutations E1064A, H1069Q, R1151H, and C1104F. J. Biol. Chem. *279*, 36363–36371.

Morth, J.P., Pedersen, B.P., Toustrup-Jensen, M.S., Sorensen, T.L., Petersen, J., Andersen, J.P., Vilsen, B., and Nissen, P. (2007). Crystal structure of the sodium-potassium pump. Nature *450*, 1043–1049.

Odermatt, A., Suter, H., Krapf, R., and Solioz, M. (1993). Primary structure of two p-type ATPases involved in copper homeostasis in *Enterococcus hirae*. J. Biol. Chem. *268*, 12775–12779.

Pedersen, B.P., Buch-Pedersen, M.J., Morth, J.P., Palmgren, M.G., and Nissen, P. (2007). Crystal structure of the plasma membrane proton pump. Nature *450*, 1111–1114.

Petris, M.J., Mercer, J.F., Culvenor, J.G., Lockhart, P., Gleeson, P.A., and Camakaris, J. (1996). Ligand-regulated transport of the Menkes copper P-type ATPase efflux pump from the Golgi apparatus to the plasma membrane: a novel mechanism of regulated trafficking. EMBO J. *15*, 6084–6095.

Pettersen, E.F., Goddard, T.D., Huang, C.C., Couch, G.S., Greenblatt, D.M., Meng, E.C., and Ferrin, T.E. (2004). UCSF Chimera–a visualization system for exploratory research and analysis. J. Comput. Chem. *25*, 1605–1612.

Pufahl, R.A., Singer, C.P., Peariso, K.L., Lin, S.-J., Schmidt, P.J., Fahrni, C.J., Cizewski Culotta, V., Penner-Han, J.E., and O'Halloran, T.V. (1997). Metal ion chaperone function of the soluble Cu(I) receptor Atx1. Science *278*, 853–856.

Rensing, C., Fan, B., Sharma, R., Mitra, B., and Rosen, B.P. (2000). CopA: an *Escherichia coli* Cu(I)-translocating P-type ATPase. Proc. Natl. Acad. Sci. U.S.A. *97*, 652–656.

Rice, W.J., Young, H.S., Martin, D.W., Sachs, J.R., and Stokes, D.L. (2001). Structure of Na^{+},K^{+}-ATPase at 11 Å resolution: comparison with Ca^{2+}-ATPase in E_1 and E_2 states. Biophys. J. *80*, 2187–2197.

Rice, W.J., Kovalishin, A., and Stokes, D.L. (2006). Role of metal-binding domains of the copper pump from *Archaeoglobus fulgidus*. Biochem. Biophys. Res. Commun. *348*, 124–131.

Sazinsky, M.H., Agarwal, S., Arguello, J.M., and Rosenzweig, A.C. (2006a). Structure of the actuator domain from the *Archaeoglobus fulgidus* Cu^{+}-ATPase. Biochemistry *45*, 9949–9955.

Sazinsky, M.H., Mandal, A.K., Arguello, J.M., and Rosenzweig, A.C. (2006b). Structure of the ATP binding domain from the *Archaeoglobus fulgidus* Cu^{+}-ATPase. J. Biol. Chem. *281*, 11161–11166.

Schaefer, M., Hopkins, R.G., Failla, M.L., and Gitlin, J.D. (1999). Hepatocyte-specific localization and copper-dependent trafficking of the Wilson's disease protein in the liver. Am. J. Physiol. *276*, G639–G646.

Sorensen, T.L., Møller, J.V., and Nissen, P. (2004). Phosphoryl transfer and calcium ion occlusion in the calcium pump. Science *304*, 1672–1675.

Stokes, D.L., Delavoie, F., Rice, W.J., Champeil, P., McIntosh, D.B., and Lacapere, J.J. (2005). Structural studies of a stabilized phosphoenzyme intermediate of Ca^{2+}-ATPase. J. Biol. Chem. *280*, 18063–18072.

Takahashi, M., Kondou, Y., and Toyoshima, C. (2007). Interdomain communication in calcium pump as revealed in the crystal structures with transmembrane inhibitors. Proc. Natl. Acad. Sci. U.S.A. *104*, 5800–5805.

Toyoshima, C., and Unwin, N. (1990). Three-dimensional structure of the acetylcholine receptor by cryoelectron microscopy and helical image reconstruction. J. Cell Biol. *111*, 2623–2635.

Toyoshima, C., and Nomura, H. (2002). Structural changes in the calcium pump accompanying the dissociation of calcium. Nature *418*, 605–611.

Toyoshima, C., and Inesi, G. (2004). Structural basis of ion pumping by Ca^{2+}-ATPase of the sarcoplasmic reticulum. Annu. Rev. Biochem. *73*, 269–292.

Toyoshima, C., and Mizutani, T. (2004). Crystal structure of the calcium pump with a bound ATP analogue. Nature *430*, 529–535.

Toyoshima, C., Yonekura, K., and Sasabe, H. (1993). Contrast transfer for frozen-hydrated specimens: II. Amplitude contrast at very low frequencies. Ultramicroscopy *48*, 165–176.

Toyoshima, C., Nakasako, M., Nomura, H., and Ogawa, H. (2000). Crystal structure of the calcium pump of sarcoplasmic reticulum at 2.6 Å resolution. Nature *405*, 647–655.

Toyoshima, C., Nomura, H., and Tsuda, T. (2004). Lumenal gating mechanism revealed in calcium pump crystal structures with phosphate analogues. Nature *432*, 361–368.

Tsivkovskii, R., MacArthur, B.C., and Lutsenko, S. (2001). The Lys1010-Lys1325 fragment of the Wilson's disease protein binds nucleotides and interacts with the N-terminal domain of this protein in a copper-dependent manner. J. Biol. Chem. *276*, 2234–2242.

Vulpe, C.D., and Packman, S. (1995). Cellular copper transport. Annu. Rev. Nutr. *15*, 293–322.

Wernimont, A.K., Huffman, D.L., Lamb, A.L., O'Halloran, T.V., and Rosenzweig, A.C. (2000). Structural basis for copper transfer by the metallochaperone for the Menkes/Wilson disease proteins. Nat. Struct. Biol. *7*, 766–771.

Williams, L.E., and Mills, R.F. (2005). P(1B)-ATPases–an ancient family of transition metal pumps with diverse functions in plants. Trends Plant Sci. *10*, 491–502.

Xu, C., Rice, W.J., He, W., and Stokes, D.L. (2002). A structural model for the catalytic cycle of Ca^{2+}-ATPase. J. Mol. Biol. *316*, 201–211.

Yoshimizu, T., Omote, H., Wakabayashi, T., Sambongi, Y., and Futai, M. (1998). Essential Cys-Pro-Cys motif of *Caenorhabditis elegans* copper transport ATPase. Biosci. Biotechnol. Biochem. *62*, 1258–1260.

Yuan, D.S., Dancis, A., and Klausner, R.D. (1997). Restriction of copper export in *Saccharomyces cerevisiae* to a late Golgi or post-Golgi compartment in the secretory pathway. J. Biol. Chem. *272*, 25787–25793.

Zhang, P., Toyoshima, C., Yonekura, K., Green, N.M., and Stokes, D.L. (1998). Structure of the calcium pump from sarcoplasmic reticulum at 8 Å resolution. Nature *392*, 835–839.